Chapter 5

Impurities

Since the discovery of high temperature superconductivity in 1986, there has been a great deal of speculation about the nature of the underdoped phase(s). An undoped cuprate is an antiferromagnetic Mott insulator. The physics of a doped Mott insulator, which must connect the antiferromagnetic and superconducting phases, is not well understood theoretically, and few other real manifestations of a doped Mott insulator have been found. Above the superconducting transition temperature T_c, underdoped materials also exhibit a mysterious "pseudogap" phase,[132, 144] where density of states is gapped and electrons may be paired but there is no bulk superconductivity.

One reason these regions of phase space remain so mysterious is that extreme underdoped cuprate crystals have proven very difficult to grow, and have not been available for experimental study. In this chapter I will discuss scanning tunneling microscopy and spectroscopy results from inhomogeneous $Bi_2Sr_2CaCu_2O_{8+\delta}$ (BSCCO) crystals which may give us access to nanometer-sized patches of extreme underdoping. In these regions, we find a notable absence of defect scattering resonances, which may indicate a novel electronic structure. The relationship of the studies in this chapter to the phase diagram of BSCCO is shown in figure 5.1.

Possible explanations for the "disappearance" of defect resonances in underdoped crystal regions include a modified Kondo effect, a loss of particle-hole symmetry, or spin-charge separation or other electron fractionalization. More mundane possibilities include convergence of the hole dopants around the impurities during crystal growth or annealing, or perhaps the impurities themselves suppress the superconducting order parameter and lower the surrounding superconducting gap.

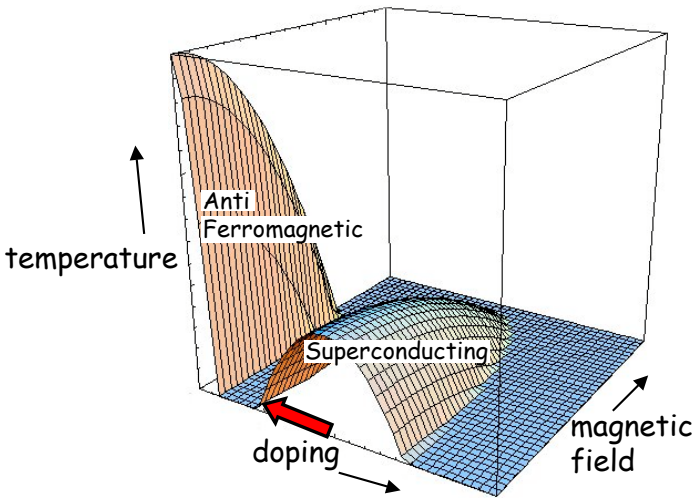

Figure 5.1: A schematic phase diagram of $Bi_2Sr_2CaCu_2O_{8+\delta}$. The red arrow shows the area in phase space covered in this chapter. Samples ranging from optimally doped to underdoped were studied at $T = 4.2$ K and $B = 0$ Tesla.

5.1 Inhomogeneity

Recently there has been much evidence for inhomogeneity in BSCCO.[91, 90, 92, 145] There has been some controversy as to whether the observed inhomogeneity is intrinsic or an artifact of dirty samples or poorly distributed oxygen atoms. Hoogenboom *et al.* claimed to have achieved homogeneity in slightly overdoped BSCCO following a specific annealing procedure, but they have never shown any 2-dimensional DOS maps to prove it. They also admit they have not been able to achieve homogeneity in underdoped BSCCO crystals.[146] Practically speaking, the apparent inevitability of inhomogeneity in underdoped crystals presents an additional challenge for bulk experimental studies: if novel properties are observed in underdoped crystals, one must ask whether they represent a single underdoped phase, or whether they are an artifact of the granularity or inhomogeneity itself. In any case, for our purposes, it matters not at all whether the inhomogeneity is an intrinsic or unavoidable phenomenon. The point is that we do see inhomogeneity in our crystals, and because we have a local probe, we can make use of the inhomogeneity to access different areas of phase space within a single crystal.

A useful way to quantify the inhomogeneity is to make a "gapmap". To do this, we measure a density of states (DOS) spectrum (101 energy points) at every single point in a 128×128 pixel, $\sim 500 \times 500$ Å field of view. From each spectrum, we extract the local gap Δ in the density of states at the Fermi level. (Note that this may or may not be a

superconducting gap; it's possible that in some spatial locations it is actually a pseudogap.)

We have measured these "gapmaps" on more than 10 different samples with nominal bulk doping ranging from $p \sim 0.1$ to $p \sim 0.17$. In all samples, we find segregation of the sample into patches of different local Δ. Each patch is 2-3 nm across. Within a typical sample, the variation in Δ from one patch to another can be as large as 100%. Example gapmaps for two samples of different bulk doping can be seen in figure 5.2.

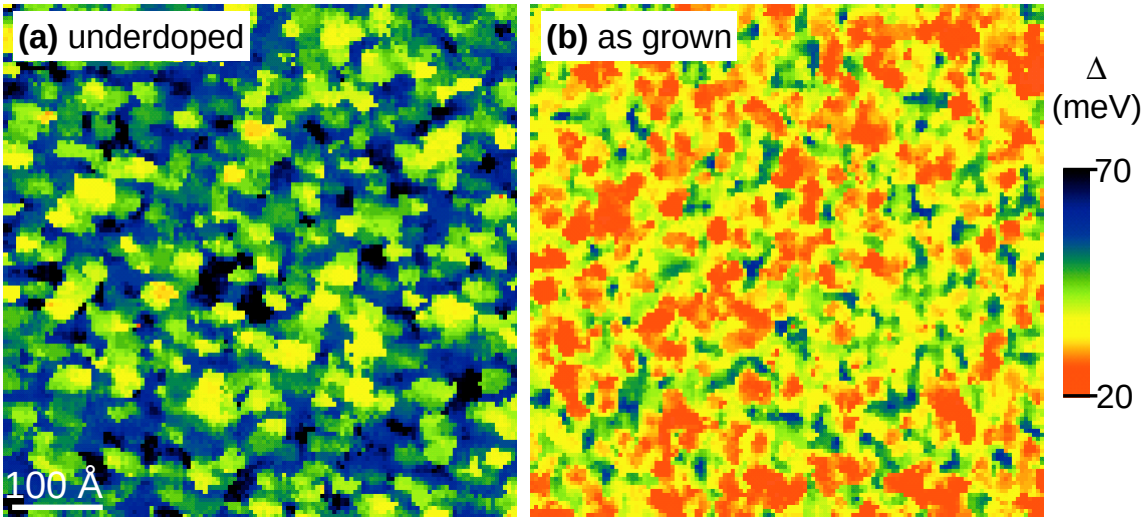

Figure 5.2: Gapmaps for (a) underdoped ($\overline{\Delta} = 50.6$ meV) BSCCO and (b) "as-grown" (slightly overdoped, $\overline{\Delta} = 35.3$ meV) BSCCO with 0.5% Ni substitutions.

Relating $\overline{\Delta}$ to T_c and p

From many different experiments on the cuprates, there are well-documented relationships between the independently controlled bulk doping p and the measured parameters T_c and mean gap of a bulk sample $\overline{\Delta}$. T_c can be related to hole concentration p using the following formula given by Presland *et al.*[147]

$$T_c/T_c^{\max} = 1 - 82.6(x - 0.16)^2 \tag{5.1}$$

This parabolic form seems to be quite general for many of the hole doped cuprates.[148] The relationship is plotted in figure 5.3(a) with $T_c^{\max} = 92$ K for optimally doped BSCCO.

Bulk mean gap $\overline{\Delta}$ can be related to hole concentration p using a compilation of measurements from SIS tunneling and ARPES. A plot from Miyakawa *et al.*[149] compiling results

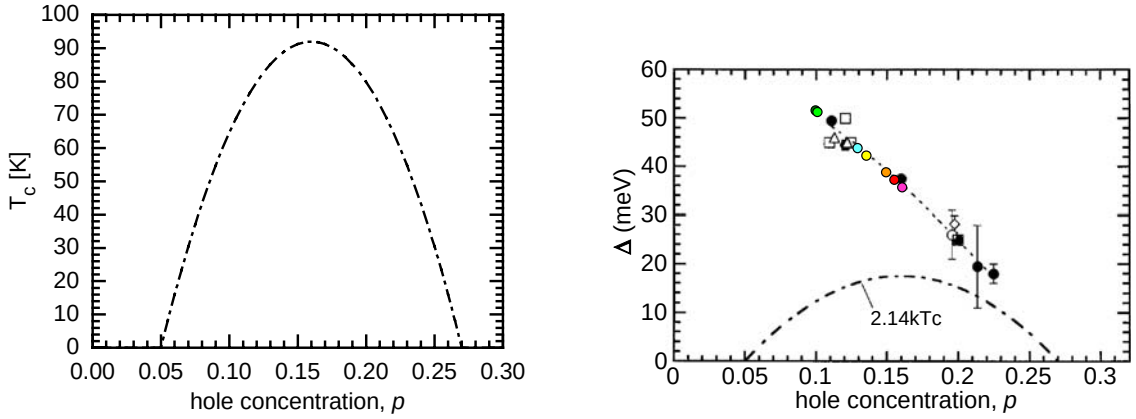

(a) T_c vs. p (b) $\overline{\Delta}$ vs. p

Figure 5.3: (a) Presland formula for critical temperature T_c vs. doping p. (b) Miyakawa plot of gap $\overline{\Delta}$ vs. doping p. Filled black circles are SIS tunneling results measured by Miyakawa *et al.*[149]; open circles and open diamonds are other SIS tunneling results; and open triangles and open squares are ARPES results. Colored circles show the measured bulk $\overline{\Delta}$ for seven different samples we have looked at. We cannot measure p directly, so I have just used our measured $\overline{\Delta}$ to place our samples onto the Miyakawa trend line.

from several experiments is reproduced here in figure 5.3(b). (Some other relevant results relating $\overline{\Delta}$ to p have been presented by Nakano *et al.*[150] and Ozyuzer *et al.*[145]) The Miyakawa plot shows a clear trend: as bulk doping p decreases, bulk $\overline{\Delta}$ increases. The best fit to the data shown by Miyakawa *et al.* gives the relationship:

$$\overline{\Delta} = 79.58 - 273.85p \tag{5.2}$$

I also plot in figure 5.3(b) colored circles representing seven of the crystals we have studied. Note that we measure $\overline{\Delta}$ but we cannot measure p directly. I have just plotted our points on top of the Miyakawa trend, with the assumption that our samples follow the same trend, so that bulk p can be estimated from the measured $\overline{\Delta}$. A summary these seven crystals is given in table 5.1.

It seems reasonable to suppose that the Miyakawa trend also holds locally in the crystal. If this is true, then a nanoscale region with low local Δ may have a high local hole concentration. Conversely, a nanoscale region with high local Δ will give us a window into the very underdoped region of the BSCCO phase diagram. As can be seen in the Miyakawa plot, the most underdoped samples available to all six different research groups who contributed data to this plot have $p \sim 0.1$ with $\overline{\Delta} \sim 50$ meV. However, in our "gapmap"

$\overline{\Delta}$ [meV] (measured, STM)	p (Miyakawa plot)	T_c (Presland formula)	T_c (measured, Eisaki)
35.3	0.163	92K	83K (0.5% Ni)
36.8	0.157	92K	85K (over)
38.9	0.150	91K	85K (0.2% Ni)
41.4	0.140	89K	84K (0.6% Zn)
43.7	0.132	86K	85K (0.2% Ni)
50.6	0.107	71K	79K (under)
50.9	0.106	70K	75K (under)

Table 5.1: Summary of measured $\overline{\Delta}$ and T_c, and calculated p and T_c for seven different crystals studied. All crystals are grown by Eisaki and Uchida, using the floating zone method. There is some disagreement between the calculated and measured T_c shown in this table. Some likely explanations for this disagreement include: (1) It is known that T_c is depressed by approximately 5 K per atomic percent by the presence of Zn or Ni impurities.[151] Therefore, the measured T_c for the Zn and Ni substituted crystals should be lower than the T_c calculated from doping p alone. (2) The T_c measurement was made by the crystal growers long before the crystals were inserted into the STM. It is possible that oxygen content changed during the long shelf time of up to several months. (3) The inhomogeneity may influence the relationship between p and T_c. If a connected path of high-T_c patches exists, then the measured bulk T_c may be higher than the average of the local T_c's from each patch.

studies, we see nanoscale patches with local gap Δ in excess of 70 meV. This indicates that with the spatial resolution of an STM we may be able to access properties of the material in a far-underdoped region of phase space inaccessible to bulk studies.

5.2 Types of Impurities

What can we learn about a new region of phase space if we have access only to a nanometer-sized patch of it? One way to probe a small region of material is to stick an impurity in, and see how the surrounding electronic structure responds. We cannot intentionally stick impurities into specific regions of the sample. But BSCCO crystals can be intentionally grown with known concentrations of impurities, so we can study the patches they happen to land in.

I will discuss three different types of impurities, all of which are centered at the Cu lattice site: intentionally substituted Zn, intentionally substituted Ni, and a native defect which

has a strong zero bias conductance peak (ZBCP). The origin of the native defect is not known for sure, but based on a combination of topographic and spectroscopic information it seems likely that it is a missing Cu atom, or a missing apical oxygen atom from directly above the Cu atom.[152] The spatial and spectroscopic signatures of these three types of impurities are shown in figure 5.4

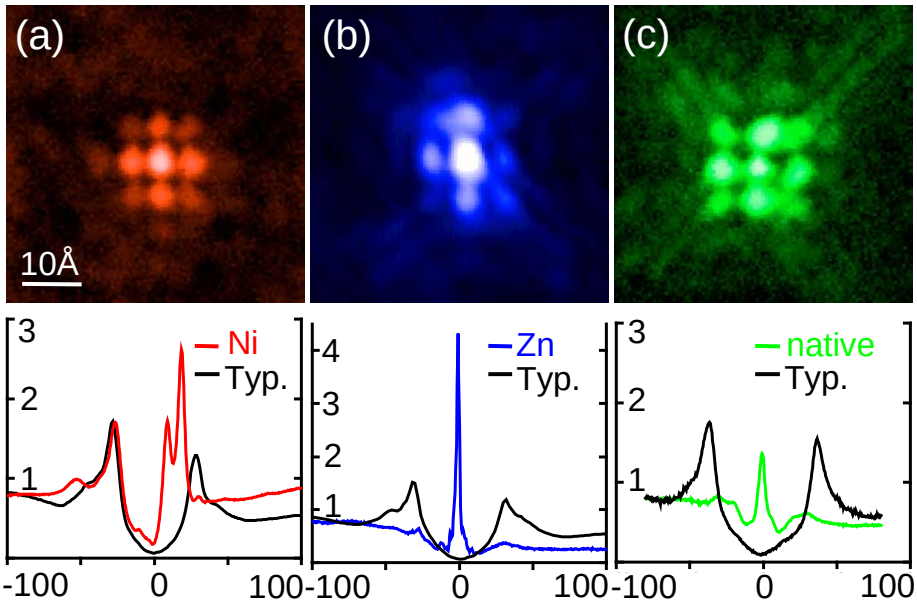

Figure 5.4: Density of states maps and spectra at (a) Ni, (b) Zn, and (c) native defect resonances in BSCCO. All maps are 50 Å square. A spectrum on the center atom of a Ni impurity shows peaks at +9 meV and +18 meV; a spectrum at a Zn impurity shows a peak at -1.5 meV; and a spectrum at a native defect shows a peak close to 0 meV. Black curves show typical spectra far from the impurities, for comparison. Each map was measured near the peak energy of the corresponding resonance: (a) +9 meV; (b) -1.5 meV; and (c) -0.5 meV.

I will report in detail on three samples:

1. nominal 0.6% Zn substitution (actual observed $\sim$ 0.13%);
   "as-grown" $T_c = 84$ K

2. nominal 0.2% Ni substitution (actual observed $\sim$ 0.21%);
   also contains $\sim$ 0.14% native defects with ZBCPs;
   "as-grown" $T_c = 85$ K

3. nominally "clean", but $\sim 0.13\%$ native defects with 4-fold symmetric ZBCPs; overdoped $T_c = 85$ K

If these impurities are randomly distributed throughout the crystal, then they will land in many different patches of different Δ. By measuring the properties of the electronic perturbations caused by these impurities as a function of their local environment Δ, we may be able to probe patches of the very far underdoped region of the crystal. The punch-line to this story is that the impurities apparently *do not even show up* in the very large Δ (or very underdoped) regions of the crystal!

5.3 Defect Properties vs. Local Δ

To catalog the properties of large numbers of defects versus their surrounding local gap, automatic algorithms are needed for (1) identifying defects; and (2) computing the local gap Δ.

5.3.1 Identifying Defects

Each type of defect produces a resonance in the density of states at a characteristic energy. One correlation to look for is dependence of the strength of this resonance on local gap Δ. Since it's possible that the resonance will be significantly weaker in some local environments than others, we need a clear-cut algorithm for distinguishing between a weak impurity and a noise spike.

It's easier to make the distinction between real defects and noise when the data has higher energy resolution and higher spatial resolution. Due to limitations in the helium hold time of the fridge, most of our datasets have only 4 Å spatial resolution and 2 meV energy resolution. (A summary of the available data resolution is shown in table 5.2.) The identification of real impurities in low spatial resolution data can be somewhat ambiguous.

Zn impurities

Zn impurities have a peak in the density of states at -1.5 meV. This peak is strongest on the central atom, and falls off to about 1/5 of the value on the next nearest neighboring atoms.[153] In order to look for Zn resonances, I plot in figure 5.6 the strength of all local maxima in the 0 meV density of states map. Of course this includes all of the local maxima

nominal impurities	spatial resolution	energy resolution
0.6% Zn	4.1 Å	2 meV
0.2% Ni	4.7 Å	2 meV
none	1.3 Å	2 meV

Table 5.2: Spatial and energy resolution available for the three samples studied in this chapter.

in the background noise too. By examination of this plot, I impose a sensible cutoff at 0.2 nS zero bias conductance. From this cutoff, I find 25 Zn impurities in a 530 × 530 Å field of view, resulting in an actual concentration of 0.13% Zn substitution.

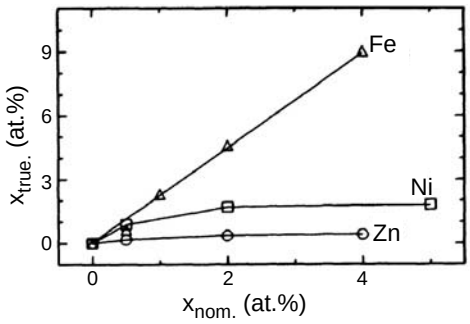

Figure 5.5: True vs. nominal impurity concentration.[151] Despite the introduction of a large number of impurities into the melt while the crystal is growing, some impurities do not incorporate well into the crystal, but are rather swept along by the melt. Therefore the true impurity concentration, measured by independent means after crystal growth, may be much less than the nominal impurity concentration, which is the % of impurities in the melt. This figure is borrowed from vom Hedt *et al.*[151]

The nominal Zn substitution was 0.6%, a factor of almost 5 higher than that observed. There are two possibilities for this discrepancy. One possibility is that the crystal actually contains fewer Zn atoms than the crystal growers thought. The crystal was grown by the floating zone method, so it is possible that most of the Zn impurity atoms introduced in the Cu mix are simply swept along instead of incorporating into the crystal. In fact, vom Hedt *et al.*[151] grew Zn-substituted BSCCO crystals by a similar method, and reported that the Zn concentration incorporated into the crystal saturated at 0.4% even as the starting Zn concentration in the melt was increased to 4%. The true impurity concentration (as measured by x-ray wavelength-dispersive microprobe analysis) is shown vs. nominal concentration in figure 5.5. According to the vom Hedt plot, our measured Zn concentration of 0.13% is very close to what we should expect for a nominal Zn concentration of 0.6%.

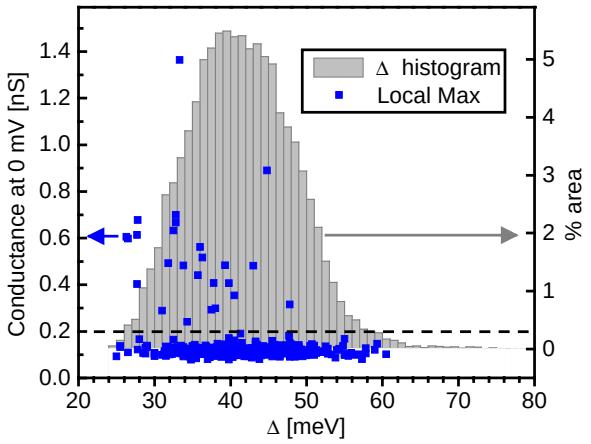

Figure 5.6: Strength of all local maxima in the 0 meV dI/dV map vs. local gap Δ, in nominal 0.6% Zn-substituted BSCCO. Over 500 local maxima are shown here as blue squares, but clearly the vast majority are just local maxima in the background noise. A sensible cutoff of 0.2 nS is imposed to separate true resonances from local noise maxima. A histogram of the gapmap values is plotted in the background in grey for comparison.

Another possibility is that more Zn impurities are present but for some reason we cannot see all of them, perhaps due to differences in their local environment which render them invisible to our STM technique. This may be true, but as we shall see, it would only account for ∼18% missing zinc atoms, not the ∼80% discrepancy we see. The most likely explanation for the bulk of the discrepancy is that the number of Zn atoms actually incorporated is significantly less than the number of Zn atoms introduced in the melt, and the "nominal" impurity concentration is simply not a reliable quantity.

Ni impurities

Ni impurities are more complicated (because they have spin 1, as opposed to Zn which has spin 0, so Ni resonance peaks are split in two). They have peaks in the density of states at +9 meV and +18 meV on the central atom, but they also have peaks in the density of states at -9 meV and -18 meV close to the nearest neighbor atoms.[154] The central atom peak is the strongest, so we look for Ni atoms in the positive density of states maps. We find Ni atoms by their +18 meV resonance (instead of their +9 meV resonance) for two reasons. First, since our sample has only 2 meV energy resolution, we would need to look for the +9 meV peak in the +8 meV or +10 meV maps, where it will not be at full strength. Second, this sample also contains a high concentration of native impurities, which have strong density of states peaks near zero bias. The tails of these strong peaks are still visible

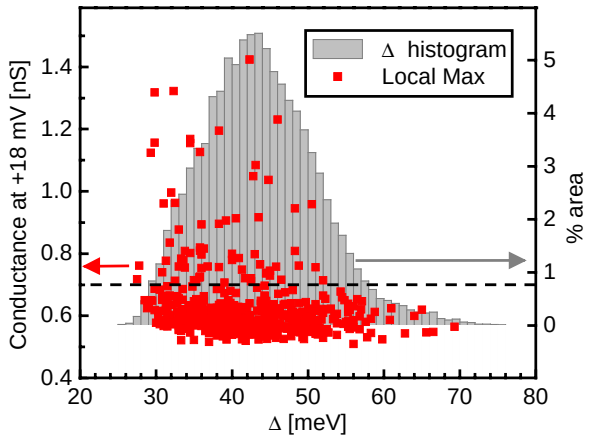

Figure 5.7: Strength of all local maxima in the +18 meV dI/dV map vs. local gap Δ, in nominal 0.2% Ni-substituted BSCCO. Over 500 local maxima are shown here as red squares, but a sensible cutoff of 0.7 nS is imposed to separate true resonances from local noise maxima. A histogram of the gapmap values is plotted in the background in grey.

as far away from zero bias as 10 meV, which makes it difficult to distinguish between Ni impurities and native impurities by looking at a +10 meV map.

The strength of all local maxima in the +18 meV map is plotted in figure 5.7. Here it is somewhat less clear where to impose a cutoff than in the Zn case. We impose a low cutoff at 0.7 nS conductance, and risk including some noise amongst our Ni resonances, rather than omit any real Ni resonances. This cutoff leads to 53 Ni resonances in the field of view. In fact, we are almost certainly including some noise, since the nominal Ni concentration is 0.2% but the observed Ni concentration is 0.21%. It's more likely that the true concentration is somewhat less than the nominal concentration, as shown in figure 5.5.

Native Defects

Unintentional native defects appear in most samples, and are similar to Zn impurities in that they have a strong peak in the density of states near zero bias. The local maxima of zero bias maps for two samples are shown in figure 5.8. Based on these plots, thresholds are imposed at 0.4 nS and 0.2 nS. (The values are somewhat different, most likely because the phase of lock-in dI/dV was set incorrectly in the 0.2% Ni-substituted map. An incorrectly set phase merely results in a constant offset in the conductance measurement. Indeed, the green value plots in figures 5.8(a) and 5.8(b) are very similar, just shifted by 0.2 nS on the vertical axis.)

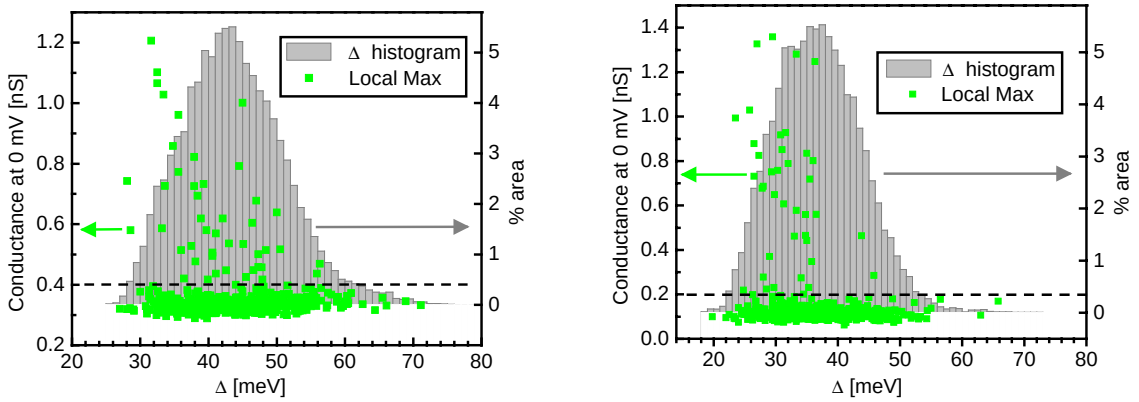

(a) nominally 0.2% Ni substitutions

(b) nominally no substitutions

Figure 5.8: Strength of all local maxima in the 0 meV dI/dV map vs. local gap Δ, in (a) nominal 0.2% Ni-substituted BSCCO, and (b) nominally clean BSCCO with no intentional impurities. Over 500 local maxima are shown here as green squares, but sensible cutoffs of (a) 0.4 nS and (b) 0.2 nS are imposed to separate true resonances from local noise maxima. Histograms of the gapmap values for the two samples are plotted in the background in grey.

The spatial pattern of the native defects is somewhat different from the Zn spatial pattern. Unlike Zn and Ni, the native defect resonance has more strength on neighboring atoms than it does on the central atom. Therefore we impose an additional constraint when looking for native impurities in the low spatial resolution dataset in figure 5.8(a). They must have two adjacent pixels with a high zero bias conductance. In figure 5.9(a), the three local maxima eliminated by this additional constraint are circled in yellow, cyan, and orange. In figure 5.9(b) spectra from these and several other local maxima are shown for comparison. It is apparent from these spectra that there is really no zero bias conductance peak in the eliminated local maxima.

The other dataset, in figure 5.8(b) has high spatial resolution, so we impose the additional constraint that observed ZBCPs must exhibit clear 4-fold symmetry in the zero bias conductance map. This eliminates 4 of the 34 local maxima which exceeded the cutoff of 0.2 nS. (All 4 eliminated had local $\Delta < 35$ meV.)

5.3.2 Local Gap Determination

The local gap needs to be determined at a large number of pixels, so it is impractical to look at every single spectra individually and determine the gap by eye. The spectra are also somewhat noisy, so the determination of gap by eye might in some cases be somewhat

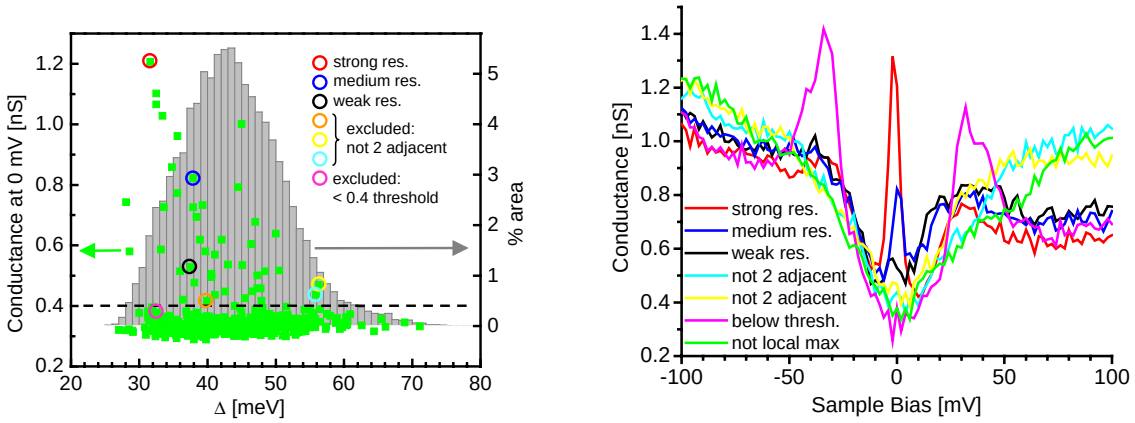

(a) local max (b) sample curves

Figure 5.9: Sample curves from potential native defect sites. In order to find the native defects, we impose two constraints: zero bias conductance must exceed a certain threshold, and the spatial signature must include two adjacent pixels with high zero bias conductance. (a) circles several definite zero bias defects and several borderline "local maxima", while (b) shows sample spectra from the chosen circles examples in (a). We can see that the automatic criteria were good; only red, blue, and black deserved to be called zero bias conductance peaks, and only these three spectra passed the automatic criteria.

subjective. This might lead to a false correlation between impurity characteristics and local gap, if the by-eye-gap-determiner really *wants* the local gap to take a certain value in order to support an attractive hypothesis.

So it is safer to let a computer algorithm do the gap determination. Of course any program is written by a human and may still be subject to systematic errors in gap determination, but at least any such errors will be systematic and objective. The computer algorithm to find the gap is summarized in appendix A. In summary, the algorithm looks for positive and negative gap-edge peaks, then returns the average, $\Delta = (\Delta_+ + \Delta_-)/2$.

Local gap around an impurity

It is important to choose a consistent method to measure the local gap around an impurity. In some cases, the impurity destroys the coherence peaks on site, so it is difficult to determine the local gap. It makes more sense to look for the gap in neighboring pixels. But how far away should we look? We could try 4 nearest neighboring pixels, 8 nearest plus next nearest neighboring pixels, 12, 20, etc. The more pixels we average over, the more likely we are to be sampling an adjacent nanoscale region with totally different local Δ.

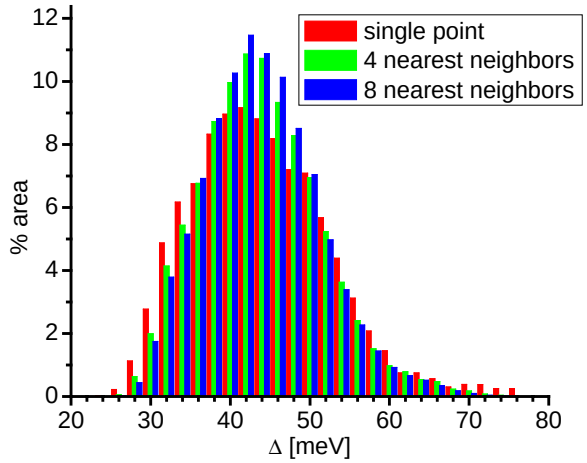

Figure 5.10: Comparison of gap histograms for different averaging schemes. Red shows the true single-pixel gap histogram, which has the largest spread. Green shows a histogram of the average of 4 nearest-neighboring pixels around each central pixel. Blue shows the average of 8 nearest-neighboring pixels; blue has all but lost the tails of the distribution.

Averaging over multiple pixels will have the effect of narrowing all gap distributions and eliminating the tails of the distributions. For example, figure 5.10 shows the histogram of local gap in a single field of view for three different averaging schemes: (red) single pixel distribution; (green) average of 4 nearest neighbors around each pixel; (blue) average of 8 nearest neighbors around each pixel. Note that the red distribution is broadest and has the longest tails, while the blue distribution has lost significant weight in the tails.

In order to define the local gap around each pixel without inadvertently including pixels from neighboring different-gapped regions, we define the local gap at a given pixel as the average of the gap measured at its four nearest neighbor pixels.

5.3.3 Distribution of Impurities

Now that we have an objective algorithm to (a) locate impurities and (b) determine the local gap Δ around the impurities, we can plot their distributions. Histograms of total gap distributions and impurity local gap distributions are shown in figure 5.11. The locations of the impurities are superimposed on the gapmaps in figure 5.12. It is striking that no defect resonances of any type appear in large gap regions any of these three samples.

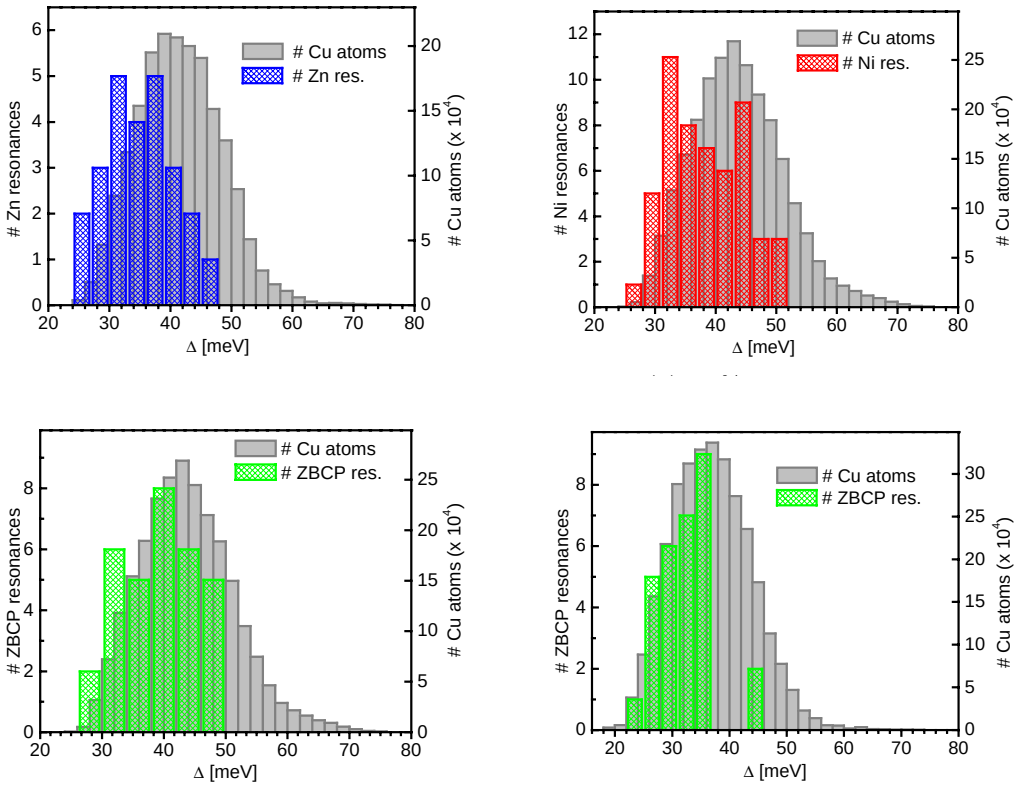

(c) 0.2% Ni substitution

(d) no intentional substitution

Figure 5.11: Gap and defect histograms. Histograms of Δ from three spectral-surveys are shown in gray. Histograms of local Δ at the impurity sites are shown in blue (Zn substitution), red (Ni substitution), and green (native defect). For each impurity resonance, the local gap is determined by the spatial average of Δ from the four nearest neighbor pixels, effectively 4 points approximately 4-5 Å away on all 4 sides. Although for $\Delta < 35$ meV the total Δ distributions and impurity site Δ distributions are similar in shape, above $\Delta \sim 35$ meV they rapidly diverge and the impurity resonance distributions reach zero by 50 meV. Remarkably, no defect scattering-resonances are observed in any region where $\Delta > 50 \pm 2$ meV.

Are these distributions a statistical accident?

With a small number of defects, statistical fluctuations might result in the absence of defects in regions where $\Delta > 50$ meV. However, if the defects are distributed randomly, and if all regions can support quasiparticle scattering resonances, our non-observation (in three independent experiments on three different crystals) of defect resonances in regions with $\Delta > \Delta_{\text{cutoff}}$ (where $\Delta_{\text{cutoff}} \sim 50$ meV) has a very low combined probability.

For each sample and impurity type, the probability of such a low-Δ distribution of

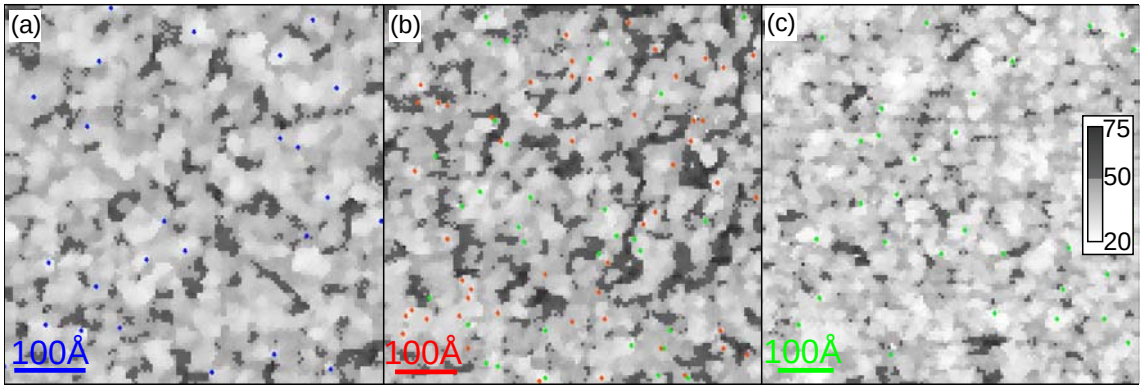

Figure 5.12: Location of defect resonances with respect to gapmap. Spectral surveys of 101 energies × 128 × 128 pixels were acquired at 4.2K on three BSCCO samples, all with tunnel junction resistance of 1GΩ. The gapmap calculated from each spectral survey is shown with a color scale such that regions with $\Delta < 50$ meV are light gray and regions with $\Delta > 50$ meV are dark gray. The locations of defect resonances are superimposed on the gapmaps in blue (Zn substitutions), red (Ni substitutions), and green (native defects). No defect resonances of any type were detected in dark gray regions where $\Delta > 50 \pm 2.5$ meV in any of the three samples.

sample	defect	# observed	Δ_{cutoff} (highest Δ at observed defect site)	% area with $\Delta < \Delta_{\text{cutoff}}$	probability of accidental occurrence
0.6% Zn	Zn	25	47.8 meV	82.4%	0.007910
0.2% Ni	Ni	53	52.0 meV	86.7%	0.000519
0.2% Ni	native	32	49.8 meV	80.4%	0.000929
"clean"	native	30	45.8 meV	90.4%	0.032339

Table 5.3: Defect resonance gap distributions and their probability of occurrence.

visible resonances is:

$$p(\Delta_{\text{imp}} < \Delta_{\text{cutoff}} \ \ \forall \ \ \text{impurities}) = (\%\ \text{area with}\ \Delta < \Delta_{\text{cutoff}})^{(\#\ \text{impurities observed})} \qquad (5.3)$$

Combining the probabilities from our 3 samples results in a total probability of:

$$p_{\text{total}} = (0.824)^{25} \times (0.867)^{53} \times (0.804)^{32} \times (0.904)^{30} = 2 \times 10^{-10}, \qquad (5.4)$$

very low indeed. However, in our excessive care to include all visible impurity resonances,

we may have inadvertently included some noise spikes. Reducing the exponents in equation 5.4 will increase p_{total}. So let us go back to figures 5.6, 5.7, and 5.8 and impose a more stringent conductance cutoff, just to see how much it might increase our chances of accidental occurrence of this low-Δ distribution. In the Zn-doped sample, the cutoff was very clear; it does not need to be changed. In the "clean" sample, each defect was simultaneously identified by its spatial pattern in a high-spatial resolution map, so the cutoff does not need to be changed. However, in the Ni-doped sample we can choose a more conservative cutoff of 0.85 nS for identification of Ni impurities, and a cutoff of 0.6 nS for identification of native defects. This results in a new total of 22 Ni impurities and 20 native defects. The new probability of these distributions occurring by chance is:

$$p_{\text{total}} = (0.824)^{25} \times (0.839)^{22} \times (0.804)^{20} \times (0.904)^{30} = 1 \times 10^{-7} \tag{5.5}$$

Therefore, with either a liberal or conservative criterion for locating defects, chance occurrence of this low-Δ distribution appears ruled out.

Are dopants attracted to defect regions during crystal growth?

One scenario which might explain our observations is that defects somehow seed nanoscale regions, influencing them to develop into superconducting domains with $\Delta < 50$ meV. Perhaps oxygen dopant atoms are attracted to the vicinity of defect sites, either during crystal growth, subsequent annealing, or mobility at room temperature during crystal storage. Even if the oxygen atoms do not move at all, it is possible that the doped holes in the CuO plane congregate near defects. These pockets of oxygen and their concomitant holes would locally depress Δ and would thus explain our observed correlation between visible defects and low-Δ regions.

This scenario seems unlikely, because visible resonances at both Ni and Zn (and possibly vacancy) sites would have to attract holes. The Cu atoms in the crystal are believed to have valance $3d^9$ and charge +2. The Ni substitutions are believed to have valance $3d^8$ and charge +2. Zn substitutions are believed to have valance $3d^{10}$ and charge +2. So there is no compelling reason why both Ni and Zn substitutions would attract oxygen atoms or holes. In fact, since they are on opposite sides of Cu in the periodic table, one might expect that if Ni attracts oxygen or holes, then Zn would repel oxygen or holes, or vice versa. Some relevant properties of Ni, Cu, and Zn are shown in table 5.4. From this it can be seen that almost all chemical properties of Cu are intermediate between the properties of Ni and Zn, so it is likely that Ni and Zn would have opposite chemical behavior with respect to Cu.

element	ionization energy (eV)			electronegativity	covalent
	1^{st}	2^{nd}	3^{rd}	(Pauling scale: 0-4)	radius (Å)
Ni	7.635	18.15	35.16	1.91	1.15
Cu	7.726	20.29	36.83	1.9	1.17
Zn	9.394	17.96	39.7	1.65	1.25

Table 5.4: Some chemical properties of Ni, Cu, and Zn which might affect their tendency to attract oxygen atoms or holes in a cuprate superconductor. For all properties listed, Cu has values intermediate between those of Ni and Zn.

In summary, attraction of dopants to Zn substitutions, Ni substitutions, and native defects is a possible scenario we cannot rule out. However, it seems unlikely because Zn and Ni sandwich Cu in the periodic table, and thus might be expected to display opposite chemical behavior, not the same behavior.

Does the impurity lower the gap in the surrounding region?

Defects of any type may suppress superconductivity and thus lower the superconducting order parameter and local gap Δ (without actually affecting local dopant concentration). One might expect that Zn (which has spin 0 and is non-magnetic) would have a more disruptive effect than Ni (which has spin 1 and is magnetic) when substituting for the magnetic spin-1/2 Cu atom. There is some conflicting literature in this regard.

Vom Hedt *et al.* report that Zn and Ni (and in fact Co and Fe too) substitutional impurities in BSCCO have exactly the same effect on T_c, which might imply that no one element is more disruptive to local superconductivity than the other. All four substitutional impurities suppress T_c with an initial slope (at low concentrations) of -5 K / atomic %, as shown in figure 5.13(a), copied from vom Hedt *et al.*[151] This slope holds up to 2% for Ni and Fe, but it has not been measured beyond 0.4% for Zn, because of difficulties in sample growth. Although the three closely spaced data points measured for Zn substitution in BSCCO may be insufficient to establish a reliable trend, the effect of Ni substitution on T_c in BSCCO has been verified by Hancotte *et al.*[155]

However, a later study by Westerholt *et al.* showed that Zn causes a much larger T_c suppression than Ni or Fe when substituted in YBCO. Here it is apparently easier to achieve high Zn concentration, and the T_c drop is 15 K / atomic % Zn, compared to ∼2 K / atomic % Ni, as shown in figure 5.13(b). Other non-magnetic elements such as Al and Mo also cause large T_c suppression, while other magnetic elements such as Fe have a weaker

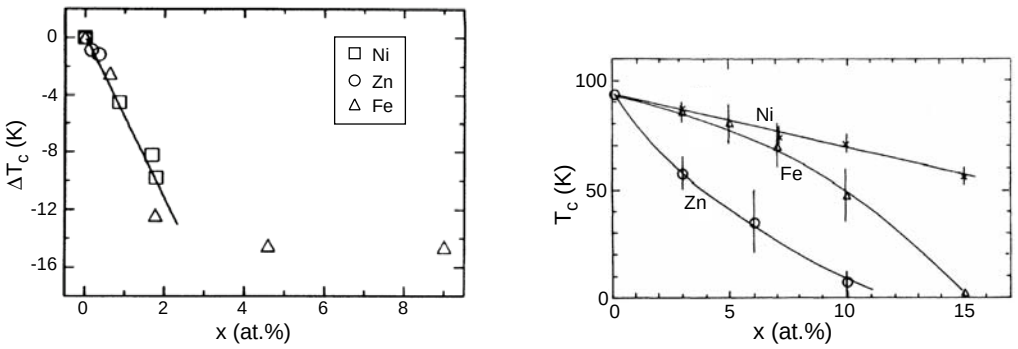

(a) $Bi_2Sr_2CaCu_2O_{8+\delta}$ (b) $YBa_2Cu_3O_{7-\delta}$

Figure 5.13: Bulk T_c suppression by substitution of Ni, Zn, or Fe impurities in BSCCO[151] or YBCO[156]

effect.[156]

Furthermore, S-I-S tunneling experiments, both STM and break junction, on Ni and Zn substituted crystals have shown that Zn concentration up to 1% has little effect on gap $\overline{\Delta}$ (if anything, $\overline{\Delta}$ decreases slightly). On the contrary, Ni substitution up to 2% increases $\overline{\Delta}$ by up to a factor of 2.[155] However, a theoretical study of Ni atoms in BSCCO requires that Ni atoms locally suppress Δ by 6 meV in order to achieve a good fit to the data.[157]

Microscopic studies show that Zn atoms locally destroy the superconducting coherence peaks.[153] Substitution of Ni at a Cu site has a much weaker effect on the local electronic structure of superconductivity. Ni atoms retain particle-hole symmetry in the electronic structure (a hallmark of superconductivity), when integrated over area. This is in stark contrast to Zn atoms which display a single resonance at -1.5 meV. Furthermore, the superconducting coherence peak is still strong at the Ni site and neighboring sites, in contrast to the coherence peaks which are destroyed surrounding the Zn site.[154]

defect	$\overline{\Delta}_{\text{total}}$ (meV)	$\overline{\Delta}_{\text{defect}}$ (meV)	abs. difference	% difference
Zn	41.4 ± 7.8	35.9 ± 5.7	5.5	13.3%
Ni	43.6 ± 8.7	38.7 ± 6.4	4.9	11.2%
native	36.8 ± 8.2	32.1 ± 4.8	4.7	12.8%

Table 5.5: Mean gap overall for three samples, and mean gap surrounding just the defects in these samples.

Therefore, while it might be reasonable to guess that Zn significantly depresses the superconducting gap, we would expect that suppression of the gap by a Ni impurity would be substantially less pronounced. However, both Zn and Ni display similar local Δ distri-

butions, as shown in table 5.5. Furthermore, impurity atoms are clearly not necessary to create patches of low Δ, since these low-Δ regions exist even in samples with no visible defects.

Does the impurity intensity decrease with increasing local gap?

It is important to distinguish whether the defect resonances are actually absent in high-Δ regions, or merely too weak to detect in the presence of noise. If the defect resonances are decreasing in strength as a function of increasing local Δ then we would expect that at some Δ_{cutoff} the resonances would drop below the noise level and we would no longer be able to detect them. However, we can see from figures 5.6, 5.7, and 5.8, that the strength of the impurity resonance does not appear to be dependent on local Δ. Furthermore, the impurity with largest detected Δ is not necessarily close to the noise level.

Are the impurities present but not visible in the high-gap regions?

The final, and most interesting, hypothesis is that Zn, Ni, and native defects are physically present in regions with $\Delta > 50$ meV, but that they do not create scattering resonances because these regions represent an electronically distinct phase. If defects are randomly distributed, and if the locations of defect resonances indicate the local existence of superconductivity, then the distribution of superconducting regions has a similar shape to the colored histograms shown in figure 5.11. The picture would then be of superconducting regions when $\Delta < 50$ meV, and an unidentified second phase (possibly the pseudogap phase) when $\Delta > 50$ meV. Data concerning typical shapes of the DOS spectra corroborates this picture[92] particularly because the energy where regions of low-Δ and sharp coherence peaks disappear is identical to the energy where the defect resonances disappear.[92] Overall, these measurements suggest BSCCO is inhomogeneous, possibly with superconducting regions embedded in an electronically distinct underdoped background.

Additional evidence: native defect concentration vs. doping

One experiment to distinguish between this chemical explanation for the correlation between visible defect resonances and low-Δ regions, and the explanation that defects are present everywhere but for some reason *invisible* in the high-Δ regions is the following: Grow a single sample with a uniform concentration of Ni or Zn substitutions. Then split the sample into several pieces and anneal each piece in different oxygen environments to

change the bulk doping of the crystal. The oxygen annealing temperatures ($\sim 500°$C) are much lower than the crystal growth temperatures ($\sim 800 - 900°$C), so the Ni or Zn impurities would be unable to move, while the oxygens would be mobile. Then perform STM mapping on all the samples. If the dopants merely congregate around the defects, then we should see the same number of defects in all crystals. But if the location of the dopants is uncorrelated to that of the defects, and defects are *invisible* in regions of high Δ, then we should see more Ni or Zn defect resonances in the overdoped crystals, and fewer in the underdoped crystals, despite the fact that all crystals were grown from the same melt and therefore actually contain the same number of defects.

We have not had the opportunity to perform this experiment, because we have not had access to such an intentionally specifically grown set of crystals. However, we have mapped "clean" samples at three different dopings. Each of these three crystals contains some of the same native defects discussed above, identifiable by a sharp zero bias conductance peak, and a characteristic four-fold symmetric spatial pattern. However, as the doping decreases, so does the number of these visible defects.

From topographic information, which shows an indentation at the defect site, we believe that these defects are some kind of missing atom, perhaps missing Cu or missing apical O. If these defects are really missing Cu atoms, we should expect that their numbers would be the same for all three crystals, since the crystals are grown first, and doped second, at a temperature too low for Cu atoms to be mobile. If the defects are missing apical oxygen atoms, we might expect that the number of defects would *increase* as we underdope and reduce the total number of oxygen atoms in the crystal. However, we see the number of defects *decrease* as we underdope.

Zero bias conductance maps and their accompanying gapmaps are shown for three samples in figure 5.14. The locations of four-fold symmetric defect resonances with ZBCPs are shown as red dots superimposed on the gapmaps.

However, there are some additional ZBCPs observed without 4-fold symmetry. Their resonances are not as strong as the 4-fold symmetric ZBCPs, and they do not have any characteristic spatial structure. It is possible that they are a different manifestation of the same underlying defect as the 4-fold symmetric ZBCPs, but lacking the d-wave symmetry of the strongly superconducting nanoscale patches. These weak ZBCPs without 4-fold symmetry will require further investigation.

One can see from table 5.6 that the concentration of 4-fold symmetric ZBCPs decreases with decreasing fraction of low-Δ area in the sample. However, the sixth column shows that even the observed concentration within the low-Δ area alone is decreasing with decreasing

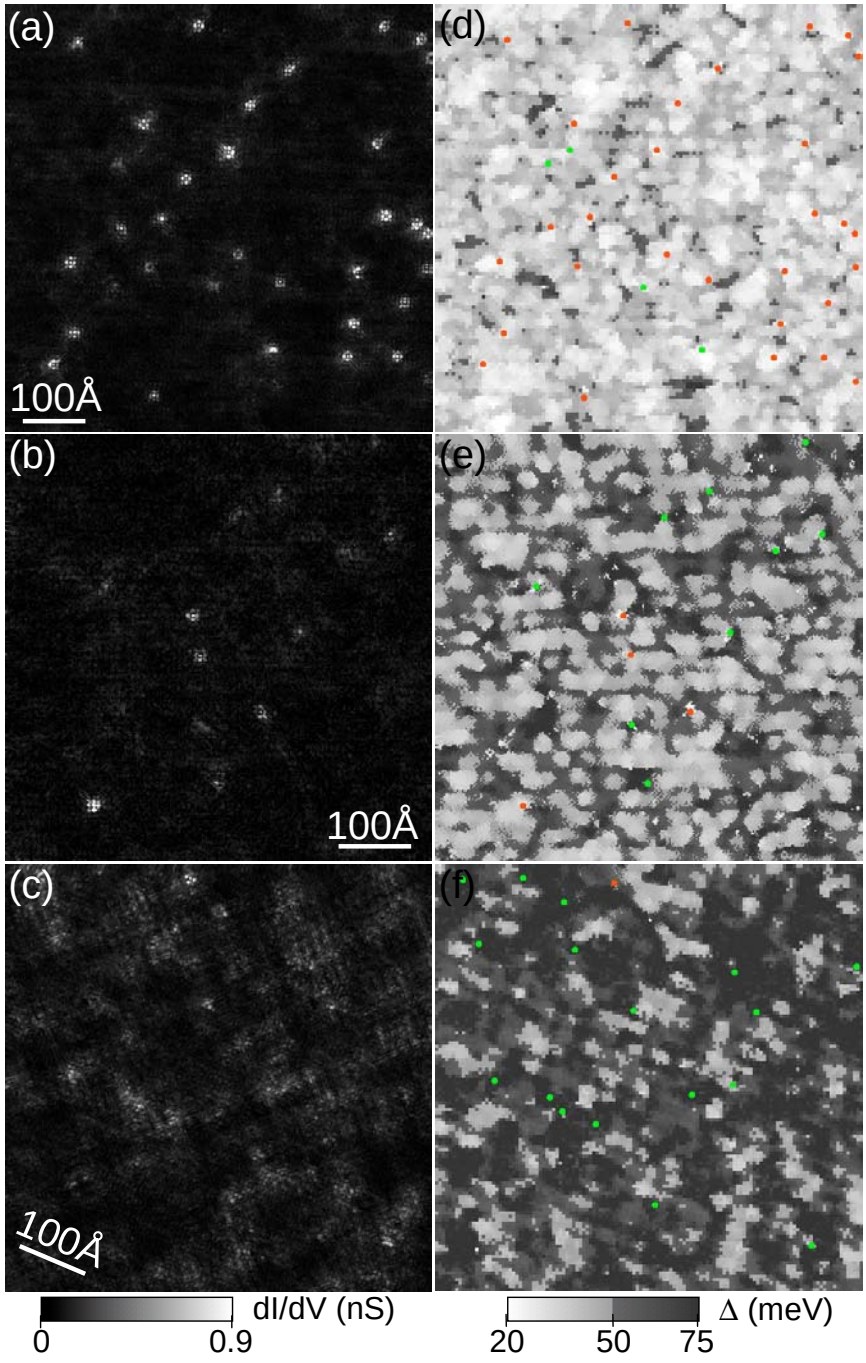

Figure 5.14: Location of defect resonances with respect to gapmap in three "clean" samples of different doping: (a) $p \sim 0.16$; (b) $p \sim 0.11$; and (c) $p \sim 0.08$. In (d)-(f), impurity locations are superimposed on gapmaps with a colorscale cutoff of ∼50 meV. Red dots represent full four-fold symmetric defects, while green dots represent weaker zero bias conductance peaks which display no four-fold symmetry. All red dots are seen in low-Δ (lightly colored) regions of the gapmaps.

sample	$\overline{\Delta}$ (meV)	% area with $\Delta < 50$ meV	4-fold symmetric ZBCPs #	4-fold symmetric ZBCPs total conc.	4-fold symmetric ZBCPs conc. in low-Δ	total ZBCPs #	total ZBCPs total conc.
85K over	36.8	94.9%	30	0.098%	0.103%	34	0.111%
75K under	50.9	53.4%	4	0.017%	0.034%	13	0.056%
65K under	62.5*	20.8%	1	0.004%	0.020%	18	0.076%

Table 5.6: Native defect resonance gap distributions and their probability of occurrence. *This value of $\overline{\Delta}$ is not reliable; the gapmap algorithm does not know how to deal with values of local $\Delta > 75$ meV, so in this very high-Δ sample, a large number of pixels were simply binned into the 75 meV bin for lack of a better plan. Thus the value 62.5 meV is likely too low.

doping. This comparison between three samples of different dopings suffers from two problems: (1) small number statistics, and (2) the unintentional nature of the impurities which prevents a more complete knowledge of their source. Although we may tentatively suppose that the decreasing number of visible 4-fold symmetric ZBCPs with decreasing doping supports the hypothesis that they only appear in low-Δ regions although they are present everywhere, we must reserve definitive judgement until a more carefully planned study with known impurities can be carried out.

5.4 Possible Theoretical Explanations

The exciting conclusion is that we can locally access patches of underdoped phase, at a doping so low that it is inaccessible to bulk studies. Numerous theoretical predictions exist for this phase, so we can for the first time begin to make comparison between theory and experiment. Some of the theories of underdoped cuprates which specifically address the nature of impurity resonances in a non-superconducting phase are summarized here.

Sachdev

Polkovnikov *et al.* explains that a non-magnetic Zn impurity in BSCCO displays a modified Kondo effect.[158] The spinless Zn replaces a spin-1/2 Cu atom, but causes a spin-1/2 moment to be distributed among the four nearest neighbor Cu atoms. NMR observations show that there is no Kondo screening of the moment at low doping.

However, Sachdev states that there is an onset of non-zero Kondo temperature T_K

at a critical doping beyond which the T_K rises rapidly. Near optimal doping, the Kondo resonance is detectable by STM as a sharp peak in the density of states whose energy and width are determined by T_K.[159]

This Kondo scenario would explain our non-observation of Zn resonances in high-Δ regions. The local doping p in the high-Δ regions is simply too low, so T_K there is less than 4.2 K. Even if there is a Zn impurity in one of these regions, there is no Kondo resonance to be seen.

Flatte

Tang and Flatté used the experimental on-site density of states spectrum at a Ni impurity to match a calculation with six adjustable but mostly independently determined parameters. They fit the chemical potential μ based on the unperturbed superconducting density of states far from a Ni impurity. Then they fit the Ni potential, both V_0 (non-magnetic) and V_S (magnetic) which set the energies of the Ni resonances at 9.2 meV and 18.6 meV. They then set the nearest-neighbor hopping δt_{01} based on the linewidth of the resonances. Finally, they must assume a local suppression of the (2-component) superconducting order parameter Δ in order to explain the energy difference between the 9.2 and 18.6 meV resonances on one side of the Fermi level, and the large peak ("coherence peak" or "van Hove singularity") on the other side of the Fermi level. The best fit for the Δ suppression is $\delta\Delta = 6$ meV, starting from an unperturbed local $\Delta = 28$ meV.[157]

A similar calculation and fit shows that a Zn impurity suppresses local Δ by $\delta\Delta = 8$ meV, starting from an unperturbed local $\Delta = 30$ meV. Missing Cu atoms should have a similar effect.[a]

If both Ni and Zn impurities are locally suppressing Δ then it makes sense that we see no Ni or Zn atoms in the highest-Δ regions. The actual shifts in the distribution $\delta\Delta = \overline{\Delta} - \overline{\Delta}_{\text{cutoff}}$ (from table 5.5) are 5.7 meV, 4.9 meV, and 4.7 meV for Zn, Ni, and native defects, respectively. These are comparable to the Tang-predicted shifts of 8 meV, 6 meV, and ∼8 meV. Therefore, according to the Tang calculation, our observation of the low-Δ distribution for impurities would be entirely explained by the local suppression of Δ by each impurity.

Flatté[160] also predicted that the resonance near the Zn impurity would be particle-hole symmetric (i.e. appearing at both -1.5 meV and +1.5 meV) for a fully phase coherent superconducting gap of 40 meV. But the resonance would lose particle-hole symmetry and

[a] Private communication from J.-M. Tang.

emphasize the -1.5 meV peak over the +1.5 meV peak if either (1) the gap became a non-superconducting "pseudogap" or (2) the superconducting gap lost phase coherence. Since we measure only the -1.5 meV peak, case (1) or (2) must be true. However, neither case predicts that the -1.5 meV resonance should disappear as well.

However, Flatté[161] has also predicted that the Ni atoms will be a local probe of superconductivity. The Ni resonance will either lose its particle hole symmetry, or disappear altogether, if placed in non-superconducting environment.

Ni atoms placed in regions where there is no pairing coherence would display only the positive energy component of their associated quasiparticles. The negative energy component, which appears only through pairing coherence, would not be visible. One can even imagine circumstances where ordinary quasiparticles found in metals, which are usually pure electron or pure hole, would lose their own coherence. For example, in the case of spin-charge separation the electron itself dissolves into two exotic particles, the 'spinon' and the 'holon'. In this event it is likely that neither an electron nor a hole component would be associated with the Ni atom.

Balatsky

Balatsky and coworkers address the DOS at a nonmagnetic impurity located in a pseudogap region. They find that the mere fact that DOS is depleted at the Fermi energy is sufficient to produce a resonance near the nonmagnetic impurity, such as Zn. While no superconductivity is required to form the impurity state in the PG, if the superconducting fluctuations are present then an additional satellite peak should appear on a symmetric bias due to the particle-hole nature of the Bogoliubov quasiparticles. The relative magnitude of the particle and the hole parts of the impurity spectrum can be used to determine the extend to which the PG is governed by the superconducting fluctuations. In the case of fully nonsuperconducting PG there should be no observable counterpart state.[162]

Their work provides impetus for the use of impurities to distinguish between local phases in cuprates. However, according to their theory, merely landing in a pseudogap region of the crystal would not cause the Zn impurity resonance to vanish, as we see. In fact, according to their theory, all of our observed Zn impurities must already be in pseudogap regions, because none exhibit the particle-hole symmetry they claim is the hallmark of an impurity in a superconductor. It's possible that the Zn impurities are so disruptive that they each locally create their own pseudogap region.

Senthil & Fisher

Senthil and Fisher provide a formal mathematical theory for fractionalization of the electron quantum number. Underdoped cuprates may have a tendency towards spin-charge separation into new quasiparticles: 'chargons' and 'spinons'. In some regions of the sample, the quasiparticles may be orthogonal to ordinary electrons so the tip electrons can't tunnel in or out because there are no overlapping states available. This means that if the defects created resonances out of these orthogonal quasiparticles, we wouldn't see them.[43]

Granular Superconductivity

Granular superconductivity occurs when microscopic superconducting grains are separated by non-superconducting regions through which Josephson tunneling between the grains establishes the macroscopic superconducting state.[163] Although crystals of the cuprate high-T_c superconductors are not granular in a structural sense, theory indicates that at low levels of hole doping the holes can become concentrated at some locations resulting in hole-rich superconducting domains.[164, 33, 165, 166] Superconductivity due to Josephson tunneling through undoped regions between such domains would represent a new paradigm for underdoped high-T_c superconductors. Since we observe three different types of defects with possibly starkly different behavior in two distinct types of sample region, it seems likely that in some bulk doping range, BSCCO is best described as a granular superconductor.

5.5 Conclusion

In conclusion, I calculated gapmaps for BSCCO samples of several different dopings, and showed that Δ is very inhomogeneous. I showed that three different types of crystal defect, Zn impurities, Ni impurities, and native defects, appear only in low-Δ regions of the crystal. This distribution is statistically significant. Although I cannot rule out a chemical explanation for this distribution, I propose that the absence of visible defect resonances in high-Δ regions is evidence for a quite different electronic phase. With a local probe such as STM, we may be able to probe nanoscale patches of the far underdoped non-superconducting phase, although bulk crystals in this doping regime are currently impossible to grow.